Applied Physics Express 7, 031101 (2014)
http://dx.doi.org/10.7567/APEX.7.031101

Reversible and nonvolatile modulation of electrical resistance in SnO_2 by external strain

Makoto Sakurai[1]*, Kewei Liu[1,2], and Masakazu Aono[1]

[1]*International Center for Materials Nanoarchitectonics (MANA), National Institute for Materials Science, Tsukuba, Ibaraki 305-0044, Japan*
[2]*State Key Laboratory of Luminescence and Applications, Changchun Institute of Optics, Fine Mechanics and Physics, Chinese Academy of Sciences, Changchun 130033, China*
E-mail: sakurai.makoto@nims.go.jp

Received December 19, 2013; accepted February 12, 2014; published online February 28, 2014

Tin oxide (SnO_2) microrods exhibited a reversible and nonvolatile semiconductor–insulator transition under an applied mechanical strain and voltage. To understand the origin of this transition, we studied the lattice defects of a SnO_2 wire under mechanical strain, using transmission electron microscopy (TEM) and photoluminescence (PL) spectroscopy. The TEM studies indicate slip planes in mechanically bent SnO_2 nanowires. The PL spectra of the bent SnO_2 microrods show strong visible emission caused by mechanical-stress-induced defects in the band gap, which supported the nonvolatile transition. © 2014 The Japan Society of Applied Physics

Nano- and macrostructured oxides have been studied intensively[1,2] and have applications in transistors,[3,4] sensors,[5–7] and photodetectors.[8–10] Defects in oxides play an important role in their electronic and optical properties,[11,12] and their effect is similar to that of impurity doping. Tin oxide (SnO_2) is one of the most promising materials for gas sensor[13] and optoelectronic applications.[14] Crystalline SnO_2 has a rutile structure and is an ideal model system for studying mechanical-strain-induced properties. This is because its structure does not have piezoelectric properties owing to its inverse symmetry. This enables one to address the features of lattice defects caused by mechanical strain. We previously demonstrated that the conductance of a single-crystal SnO_2 microrod on a flexible substrate changed between semiconducting and insulating states upon the application of mechanical strain (from bending the substrate) and an appropriate voltage.[15] The Raman spectra indicated the creation and elimination of lattice defects during the transition.

Here, we study the mechanical-strain-induced lattice defects in SnO_2 using transmission electron microscopy (TEM) and photoluminescence (PL) spectroscopy. TEM images of mechanically bent SnO_2 nanowires indicated the presence of slip planes and dislocation. The increase in the broad visible emission intensity in the PL spectra demonstrated an increase in lattice defects in the bent SnO_2 microrod. We discuss the origin of the mechanical-strain-induced transition from the semiconducting state to the insulating state in SnO_2.

SnO_2 microrods were synthesized by chemical vapor deposition.[15] The furnace temperature was kept at 990 °C for 60 min, with a flow of Ar containing 4% O_2 as a carrier gas. SnO_2 microrods with square cross sections 1–2 μm wide and 3–5 mm long were grown at the end of a ceramic boat. Metal catalysts were not required for their growth. The as-grown microrods are n-type semiconductors, with a resistivity of ~10 Ω cm. For SnO_2 nanowire growth, a sapphire substrate was placed near the source boat in the furnace. The substrate surface was covered by Au layers 4 nm thick, which acted as a catalyst, in a process similar to the growth of ZnO nanowires.[4]

The resistance of a single-crystal SnO_2 microrod on a flexible polyimide substrate was measured as a function of the strain, under a voltage (V_b) applied between electrodes spaced at 120 μm at 300 K.[15] A mechanical strain was applied from the backside of the substrate [see inset of Fig. 1(a)] using a linear positioner derived from a stepping motor (Sigma-Koki SPSG15-10). The microrod exhibited a reversible, nonvolatile transition between the semiconducting and insulating states as a function of the strain at $V_b = 6$ V, as shown in Fig. 1(a). Increasing the strain caused the resistance of the microrod to increase gradually before eventually reaching the instrumental limitation. Free electrons in the SnO_2 microrod were trapped at defect sites,[16] increasing the resistance. In the small strain region ($\varepsilon \lesssim 3\%$), the microrod regained the original value after the strain was released. The state with a reversible strain response and a resistance of 10^6–10^7 Ω (due to intrinsic defects and a few strain-induced defects) is referred to as the semiconducting state. When the strain exceeded the threshold strain, marked by a red arrow in Fig. 1(a), the microrod reached the instrumental limitation and showed a nonvolatile response to the applied strain. This

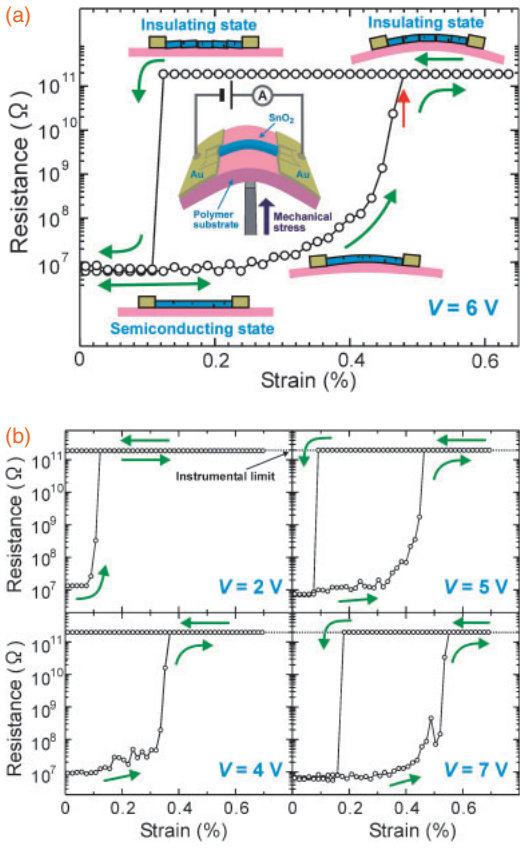

Fig. 1. (a) Resistance of SnO_2 microrod-based device as a function of strain at $V_b = 6$ V at 300 K. Inset schematically shows SnO_2 microrod device on flexible polyimide substrate under applied mechanical strain. Red arrow indicates threshold strain of semiconducting-to-insulating transition. (b) Strain vs resistance curves for the device at $V_b = 2$, 4, 5, and 7 V.

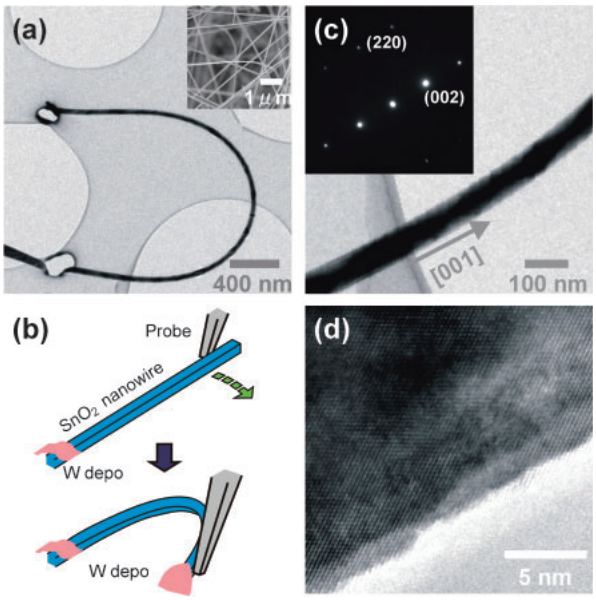

Fig. 2. (a) TEM image of bent SnO_2 nanowire on carbon TEM grid. Inset shows scanning electron microscopy image of as-grown SnO_2 nanowires. (b) Schematic showing fabrication of bent nanowires using sharp metal probe and localized tungsten deposition in FIB system. (c) TEM image of SnO_2 nanowire near fixed position on carbon TEM sheet. Inset shows diffraction pattern of nanowire. (d) High-magnification TEM image of outer surface of nanowire, where the tensile stress was weak.

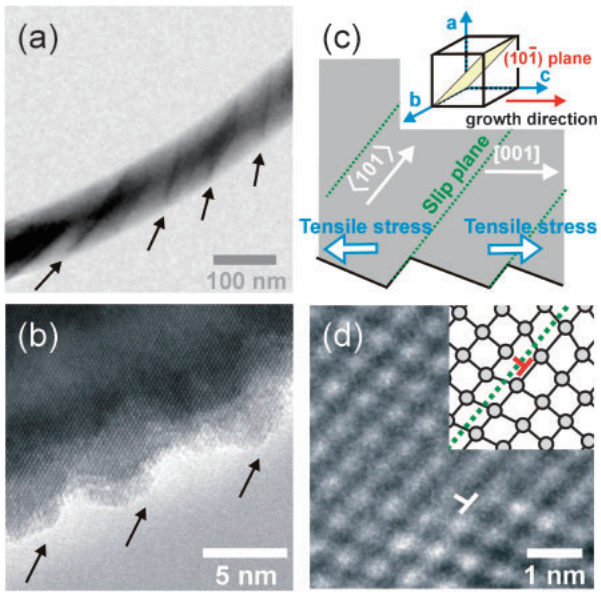

Fig. 3. (a) TEM image of bent SnO_2 nanowire under strain of ~3%. Black stripes in nanowire are marked by arrows. (b) High-magnification TEM image of outer surface under tensile strain. Arrows indicate step-like surface structures. (c) Schematic showing slip planes formed by tensile strain. Inset shows geometric relationship between [001] growth direction and (10$\bar{1}$) plane in rutile structures. (d) High-magnification TEM image of SnO_2 nanowire with dislocation under tensile strain. Inset schematically shows dislocation on slip plane.

state is referred to as the insulating state. Reducing the strain applied to the microrod in the insulating state caused it to revert to the semiconducting state at a strain of 0.12%. Figure 1(b) shows the hysteresis loops of the microrod as a function of the strain under different applied voltages. The threshold strain increased with increasing applied voltage, as shown in Fig. 1. This suggests that local Joule heating healed the lattice defects under strain, and that the healing efficiency increased with increasing electric power. Additionally, the slower transition from the semiconducting state to the insulating state with a higher applied voltage confirmed the complete creation and elimination of the defects by the application of the strain and voltage, respectively. When the strain applied to the microrod in the insulating state was reduced, the insulating state was retained at $V_b = 2$ and 4 V, even after the stress was completely released. When $V_b \geqq 5$ V was applied, the insulating state changed to the semiconducting state during the strain reduction.

To study the lattice defects caused by mechanical strain, we investigated SnO_2 nanowires instead of microrods using TEM (JEOL JEM-2100F), as shown in the inset of Fig. 2(a). The reason is that it is difficult for electrons accelerated in conventional TEM to pass through SnO_2 microrods of thickness >1 μm. After a single SnO_2 nanowire of 100 nm in diameter was placed on the TEM holder, the nanowire was bent mechanically using a combined system consisting of a focused ion beam (FIB) microscope and nanoscale manipulator (Hitachi NB5000). This is illustrated schematically in Fig. 2(b). Figure 2(a) shows a low-magnification TEM image of a bent SnO_2 nanowire on a thin carbon TEM grid. Holes at both ends of the nanowire were formed by localized tungsten deposition from the FIB system to fix the nanowire on the sheet. Tensile and compressive strain were applied to the outer and inner sides of the nanowire fixed at both ends, respectively. Figure 2(c) shows a TEM image of the SnO_2 nanowire near the fixed position in Fig. 2(a), where the stress was very weak. The diffraction pattern shown in the inset of Fig. 2(c) indicates that the nanowire grew in the [001] direction. Figure 2(d) shows a magnified TEM image of the outer surface of the SnO_2 nanowire shown in Fig. 2(c). Figure 2(d) suggests that the topography of the surface was the same as that of the as-grown nanowire without stress.

Figure 3(a) shows a TEM image of the center of the bent SnO_2 nanowire. A strain of ~3% was applied to the outside of the nanowire. Some dark stripes appeared on the bent nanowire, as marked by the arrows, which suggest lattice deformation and varying thickness within the nanowire. This was caused by the internal strain because the stripes were not observed in TEM images of straight SnO_2 nanowires. The dark stripes were aligned at an angle of ~45° with respect to the long wire direction. Figure 3(b) shows a magnified TEM image of the outer surface of the nanowire, where tensile stress was applied. Step-like structures were observed on the surface. The surface topography differed from that of the straight region shown in Fig. 2(d). Split planes in rutile structures occur mainly along the ⟨101⟩{10$\bar{1}$} plane, as shown schematically in the inset of Fig. 3(c), and the [001]{110} plane.[17–19] The step is thought to be caused by slip along the ⟨101⟩{10$\bar{1}$} plane under the applied tensile strain, as shown schematically in Fig. 3(c). Slip planes are formed by dislocation along a preferred direction of a crystal, so lattice defects tend to be created on the slip plane and be distributed locally about the plane. The present results for the nanowire suggest the creation of slip planes for a single-crystal SnO_2 microrod under tensile strain. The dislocation shown in the high-resolution TEM image [Fig. 3(d)] was thought to be created

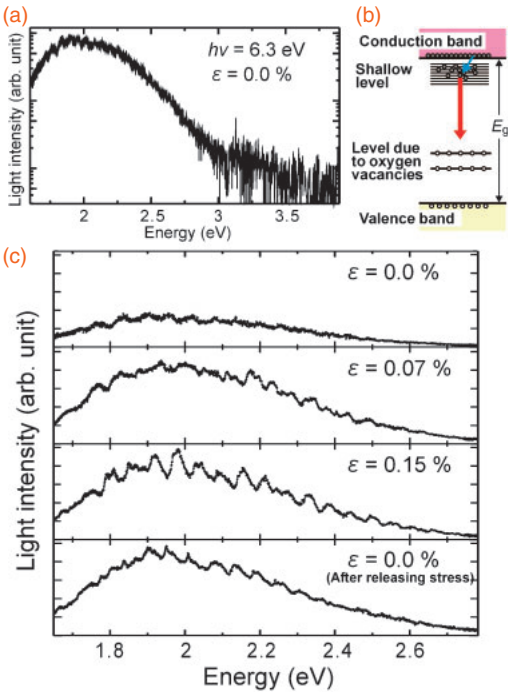

Fig. 4. (a) PL spectrum of as-grown single SnO_2 microrod at 300 K. (b) Schematic band diagram of SnO_2 with donor levels caused mainly by impurities and acceptor levels due to oxygen vacancies. (c) PL spectra of single SnO_2 microrod at different strain states. $\varepsilon = 0\%$ in the top and bottom figures corresponds to microrod before strain was applied and after it was released, respectively.

on the slip plane as a result of the mechanical strain. This situation is shown schematically in the inset of Fig. 3(d). Very few dislocations were observed in the TEM image because dislocations created locally on the slip plane do not meet the following requirement: A clear image of dislocations in TEM observations requires propagation of the dislocation from the top to the bottom of a nanowire with a thickness of: 100 nm in the direction parallel to the incident electrons.

Figure 4(a) shows a typical PL spectrum of a single SnO_2 microrod obtained with an excitation source of 6.3 eV at 300 K. There is no main peak caused by direct electron–hole recombination across the band gap ($E_g \simeq 3.6$ eV at $T = 300$ K) in SnO_2. This is because carriers excited to the conduction band quickly decay to the levels caused by impurities and defects in an as-grown microrod.[20] The broad visible emission in Fig. 4(a) was due to the radiative electron–hole recombination between the donor and acceptor levels, in which the acceptor levels are formed mainly by oxygen vacancies.[21] The defect levels in the band gap are shown schematically in Fig. 4(b). Figure 4(c) shows PL spectra of SnO_2 microrods under different strains. The top panel of Fig. 4(c) corresponds to the spectrum of an as-grown SnO_2 microrod without strain. The second and third panels show the spectra of the microrod under strains of 0.07 and 0.15%, respectively. The fourth panel was obtained from the microrod after the strain was released. Under the applied strain, the light intensity was about two to three times higher than that of the original SnO_2 microrod without strain. Satellite peaks within the broad emission band become pronounced with increasing strain. The energy difference between neighboring peaks in the visible emission is about 300–600 meV and corresponds to energy separation of the defect levels. The satellite peaks obtained at 300 K differ from those related to the longitudinal optical phonon replica observed near the main peak in low-temperature PL.[22] Each transition originated from recombination between the donor and acceptor levels, so the enhanced intensity indicated the creation of defect levels in the band gap. A similar enhancement was reported in SnO_2 nanowires with an increase in the number of oxygen vacancies under heat treatment.[23,24] The high intensity of the visible emission was retained by the microrod after the strain was released ($\varepsilon = 0$), suggesting that residual lattice defects existed within the microrod. This is consistent with the nonvolatile behavior observed in the transport measurements shown in Fig. 1.

In conclusion, mechanical strain on a SnO_2 nanowire grown in the [001] direction created slip planes that were aligned at an angle of ~45° with respect to the long wire direction. Lattice defects caused by mechanical strain produced many defect levels in the band gap of SnO_2. Some lattice defects created in the microrod by the application of strain were nonvolatile with respect to the strain. The application of mechanical strain to nano- and microscale oxide structures produces interesting functionalities via mechanical-stress-induced defect engineering. This hints at new applications and future semiconductor technologies.

Acknowledgments The work was supported in part by the World Premier International Research Center (WPI) Initiative on Materials Nanoarchitectonics, MEXT, Japan, and in part by JSPS KAKENHI (23560032). We thank Dr. S. Shimomura and Dr. K. Miyazawa of NIMS for operation of the FIB, Dr. K. Kurashima and Dr. I. Yamada of NIMS for the TEM measurements, and Dr. K. Watanabe of NIMS for measurement of the PL spectra.

1) M. H. Huang, S. Mao, H. Feick, H. Yan, Y. Wu, H. Kind, E. Weber, R. Russo, and P. Yang, Science **292**, 1897 (2001).
2) T. Zhai, X. Fang, M. Liao, X. Xu, H. Zeng, Y. Bando, and D. Golberg, Sensors **9**, 6504 (2009).
3) M. L. Lee, E. A. Fitzgerald, M. T. Bulsara, M. T. Currie, and A. Lochtefeld, J. Appl. Phys. **97**, 01101 (2005).
4) M. Sakurai, Y. G. Wang, T. Uemura, and M. Aono, Nanotechnology **20**, 155203 (2009).
5) Y. Hu, Y. Chang, P. Fei, R. L. Snyder, and Z. L. Wang, ACS Nano **4**, 1234 (2010).
6) K. Liu, M. Sakurai, and M. Aono, Sensors **10**, 8604 (2010).
7) K. Liu, M. Sakurai, and M. Aono, J. Mater. Chem. **22**, 12882 (2012).
8) P.-T. Liu, Y.-T. Chou, and L.-F. Teng, Appl. Phys. Lett. **94**, 242101 (2009).
9) H.-Y. Lee, B.-K. Wu, and M.-Y. Chern, Appl. Phys. Express **6**, 054103 (2013).
10) K. Liu, M. Sakurai, M. Liao, and M. Aono, J. Phys. Chem. C **114**, 19835 (2010).
11) S. B. Ogale, Adv. Mater. **22**, 3125 (2010).
12) H. L. Tuller and S. R. Bishop, Annu. Rev. Mater. Res. **41**, 369 (2011).
13) N. Yamazoe, Sens. Actuators B **5**, 7 (1991).
14) R. Latz, K. Michael, and M. Scherer, Jpn. J. Appl. Phys. **30**, L149 (1991).
15) K. Liu, M. Sakurai, and M. Aono, ACS Nano **6**, 7209 (2012).
16) J. E. Dominguez, L. Fu, and X. Q. Pan, Appl. Phys. Lett. **81**, 5168 (2002).
17) M. G. Blanchin and G. Fontaine, Phys. Status Solidi A **29**, 491 (1975).
18) K. H. G. Ashbee and R. E. Smallman, Proc. R. Soc. London, Ser. A **274**, 195 (1963).
19) K. H. G. Ashbee and R. E. Smallman, J. Am. Ceram. Soc. **46**, 211 (1963).
20) A. Othonos, M. Zervos, and D. Tsokkou, Nanoscale Res. Lett. **4**, 828 (2009).
21) A. Kar, S. Kundu, and A. Patra, J. Phys. Chem. C **115**, 118 (2011).
22) R. Chen, G. Z. Xing, J. Gao, Z. Zhang, T. Wu, and H. D. Sun, Appl. Phys. Lett. **95**, 061908 (2009).
23) J. Jeong, S.-P. Choi, C. I. Chang, D. C. Shin, J. S. Park, B.-T. Lee, Y.-J. Park, and H.-J. Song, Solid State Commun. **127**, 595 (2003).
24) J. X. Zhou, M. S. Zhang, J. M. Hong, and Z. Yin, Solid State Commun. **138**, 242 (2006).